Duong et al. Journal of the European Optical Society-Rapid Publications (2018) 14:25
https://doi.org/10.1186/s41476-018-0092-x

Journal of the European Optical Society-Rapid Publications

RESEARCH Open Access

Suppression of residual amplitude modulation appeared in commercial electro-optic modulator to improve iodine-frequency-stabilized laser diode using frequency modulation spectroscopy

Quang Anh Duong[1], Thanh Dong Nguyen[1], Thanh Tung Vu[2], Masato Higuchi[1], Dong Wei[1] and Masato Aketagawa[1*]

Abstract

Background: This paper shows how to suppress residual amplitude modulation (RAM) appeared in a commercial electro-optic modulator (EOM) to improve an iodine-frequency-stabilized laser diode (LD) using frequency modulation spectroscopy (FMS). Since the RAM of an EOM is affected by the temperature of the EOM, the DC-offset applied to the EOM and the polarization of the incident beam, it should easily fluctuate with drifts in temperature, applied voltage, and polarization. The fluctuation of the RAM of the EOM, which might decrease the frequency stability of the iodine-frequency-stabilized LD, must be eliminated by some means.

Methods: In this paper, we present a theoretical analysis and experimental results to express the RAM error from the EOM in a LD frequency stabilization system near 633 nm using iodine-saturated absorption. A RAM compensation system, which actuates the temperature of the EOM and the DC-offset applied to the EOM, is constructed for the commercial EOM.

Results: Using the RAM compensation system, the RAM is reduced to 10^{-4} order, and frequency stability of $\sim 3.67 \times 10^{-11}$ for 1000 s is achieved for the LD.

Conclusions: The proposed method can be applied for normal frequency stabilizing LDs, which use a commercial EOM and a low modulation index with FMS.

Keywords: Sinusoidal phase modulation, Frequency stabilization, Residual amplitude modulation, Laser diode

Introduction

Laser diodes (LDs) have become popular light sources for optical interferometers and other optical applications in the fields of high-precision engineering. With the advantages of high power, long lifetime, and small size, LDs can replace conventional gas lasers in many optical applications. Various types of LD such as inexpensive normal LDs, and tunable LDs with a narrow linewidth including an external cavity LD (ECLD), a distributed Bragg reflector (DBR) LD and a distributed feedback (DFB) LD, have been developed. In particular, to apply tunable LDs with a narrow linewidth as the light sources of precise optical interferometers whose measurable range and resolution are larger than 1 m and less than sub-nanometer order, respectively, the frequency stabilization of the LD to less than 10^{-11} is required. To stabilize the LD frequency, the linear or saturated absorption of some atomic-molecular species, such as iodine molecules, rubidium atoms, and Cs atoms [1–3], can be utilized. Sinusoidal phase/frequency modulations (SPM/SFM) and demodulation by a lock-in amplifier (LIA) are effective techniques applied to detect the

* Correspondence: masatoaa@vos.nagaokaut.ac.jp
[1]Department of Mechanical Engineering, Nagaoka University of Technology, 1603-1 Kamitomioka, Nagaoka, Niigata 940-2188, Japan
Full list of author information is available at the end of the article

atomic or molecular absorption lines for LD frequency stabilization [4–6].

Many researchers have developed methods of stabilizing the LD frequency to some atomic-molecular absorption lines. Vu et al. performed LD frequency stabilization using both a regular LD with linear absorption [5] and an ECLD with saturated absorption [6] of iodine molecules. Some of the authors of this paper also used SPM with a fixed modulation index of 3.768 rad to detect iodine-saturated absorption and stabilize the ECLD frequency for a Mach–Zehnder displacement measuring interferometer [4]. In such research [4], SPM by an electro-optic modulator (EOM) and frequency modulation spectroscopy (FMS) [7, 8] with an acousto-optic modulator (AOM) are utilized for LD frequency stabilization. The LD frequency is stabilized to an iodine-saturated absorption line near 633 nm using a null method [4]. However, owing to the residual amplitude modulation (RAM) error of the EOM [9, 10], the frequency stabilization is limited to $\sim 1 \times 10^{-10}$ for an integration time of 1000s [4]. Modulation transfer spectroscopy (MTS) [11, 12] can reduce frequency instability due to linear absorption compared to FMS. However, the RAM effect cannot be neglected for both FMS [13] and MTS [14]. Even if a high-power laser source and a long absorption cell were utilized with MTS, RAM suppression was still required to obtain high frequency stability [15].

To apply a direct phase determination method with a phase lock loop [16, 17] to the Mach–Zehnder displacement measuring interferometer appeared in [4], the modulation index should be fixed to 3.768 rad. The purpose of this paper to show an active suppression method of residual amplitude modulation appeared in a commercial electro-optic modulator with a constant modulation index of 3.768 rad, even though FMS, which is easily sensitive to linear absorption and RAM, is utilized in the frequency stabilization system. In this paper, the effects of the RAM error of the EOM on the iodine-frequency-stabilized LD at a low modulation index of 3.768 rad are examined, and some experiments performed are discussed to confirm the stability of the LD with and without the RAM error. The primary error of RAM is known to occur as the result of an etalon effect inside the EOM crystal, which is caused by the matching error between the laser beam polarization axis and the crystal axis [9]. The RAM caused by the etalon effect is a sinusoidal error with the same frequency of the phase modulation. The other causes of noise such as vibration, spatial inhomogeneity, and RF amplitude fluctuation [9, 18], which do not contain modulation frequency, are removed in demodulation with a lock-in amplifier (LIA). Many methods have been developed to eliminate the RAM error such as a two-tone method for heterodyne spectroscopy with LDs [19], harmonic frequency modulation for FMS [20], and feedback compensation of the RAM with DC-offset or temperature control [9, 18]. Reference [21] shows that a custom-designed EOM with a Brewster angle crystal is effective for suppressing the RAM. In this study, we combined the two methods of temperature and DC-offset control for a commercial EOM to eliminate the RAM error from 10^{-2} to 10^{-4} order. Finally, with RAM compensation, the frequency stability of the LD is shown to reach $\sim 3.67 \times 10^{-11}$ for 1000 s, by a beat-note measurement with a commercial iodine-stabilized He-Ne laser (frequency uncertainty $\sim 2.5 \times 10^{-11}$ [22]). The RAM suppression system is required for frequency stabilization of normal LDs, if FMS is applied to the stabilization system. And this frequency stability is sufficient for the most common applications, including a Mach–Zehnder displacement measuring interferometer [4].

Methods

Frequency modulation spectroscopy

To use a LD as the light source of a high-precision optical interferometer, it is effective to tune the LD frequency to frequency standards, which are traceable to the meter definition, such as the iodine-saturated absorption line near 633 nm [23]. In this study, SPM and FMS are employed to detect and stabilize the LD frequency to an iodine-saturated absorption line.

Figure 1 shows the FMS setup, which uses both an EOM and an AOM. The laser from the LD is split into a pump beam, which is chopped by the AOM with a square signal, and a probe beam, which is phase-modulated by the EOM. Even if there is frequency shift in the pump beam by the AOM, the AOM can be employed to chop the pump beam for detecting the Doppler-free saturated absorption [8, 24]. Since the two beams are collimated and matched with each other inside the iodine cell, the probe beam generates a saturated absorption signal that is detected by a photodetector and the first-derivative signal of the absorption that is detected by a mixer and LIA. The chopped signal by the AOM is utilized to the LIA for demodulating the absorption signal and eliminating the Doppler background [8]. And the first-derivative signal is used as an error signal by a proportional–integral–derivative (PID) controller to stabilize the LD frequency by adjusting the injection current of the LD. Using SPM, the probe beam from the LD is modulated by the sinusoidal signal $\sin\omega_m t$ (ω_m: modulation angular frequency) that drives the EOM, while the pump beam is chopped by the AOM [4]. The electrical field of the modulated probe beam is

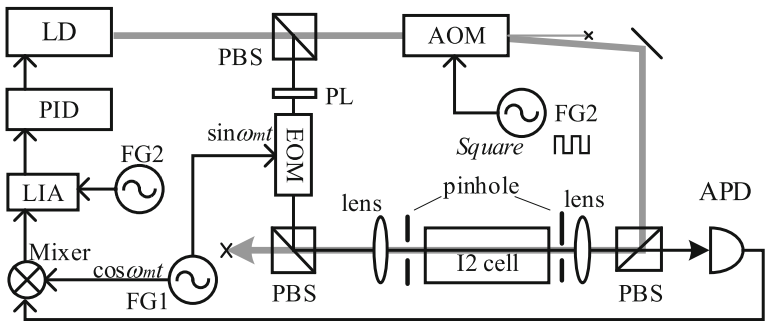

Fig. 1 Frequency modulation spectroscopy with an EOM and an AOM. LD: laser diode; FG: function generator; PL: polarizer; EOM: electro-optic modulator; AOM: acousto-optic modulator; PBS: polarizing beam splitter; APD: avalanche photodetector; PID: proportional–integral–derivative controller; LIA: lock-in amplifier

$$E_{EOM} = E_0 \exp[-i(\omega_0 t + m \sin\omega_m t)] = E_0 \sum_{k=-\infty}^{\infty} J_k(m) \exp[-i(\omega_0 + k\omega_m)t], \quad (1)$$

where E_0, ω_0, m, ω_m, and $J_k(m)$ are the electrical field amplitude, laser angular frequency, modulation index, modulated angular frequency, and the kth-order Bessel function of the modulation index (k is an integer), respectively. The phase-modulated electrical field contains many sideband components.

The pump beam is sent through the iodine molecules to create a saturated environment, where the molecules absorb the incoming photons at specific frequencies and become excited. Then, the probe beam passes through the saturated environment but cannot be absorbed by these molecules, resulting in an increase in intensity at these frequencies, which are the so-called saturated absorption lines. If the saturated absorption angular frequency of the iodine molecules is Ω, the laser absorption intensity nearby the kth sideband angular frequency ($\omega_k = \omega_0 + k\omega_m$) is [25]

$$T_{(\omega_k)} = \exp(-\delta_k - i\phi_k), \quad (2)$$

with

$$\delta_k = \frac{A.\omega_{FWHM}^2}{(\omega_k - \Omega)^2 + \omega_{FWHM}^2}, \quad (3)$$

$$\phi_k = n_k L_{cell} \frac{\omega_k}{c}, \quad (4)$$

where δ_k, ϕ_k, A, ω_{FWHM}, n_k, L_{cell}, and c are the kth-sideband amplitude attenuation, the kth-sideband phase shift, absorption amplitude, full width at half maximum angular frequency, refractive index for ω_k, iodine cell length, and light speed in vacuum, respectively.

Combining the Bessel explanation of Eqs. (1) and (2), the electrical field of the laser beam absorbed by the iodine molecules is

$$E_{trans} = E_0 \sum_{k=-\infty}^{\infty} J_k(m) \times T_{(\omega_k)} \times \exp[-i(\omega_0 + k\omega_m)t]. \quad (5)$$

The absorption signal can be detected by a photodetector (PD) placed after the iodine cell and is expressed as

$$I_{PD} = E_0^2 \times \left\{ \begin{array}{c} J_0^2(m)e^{-2\delta_0} + \sum_{k=1}^{\infty} J_k^2(m)\left(e^{-2\delta_k} + e^{-2\delta_{-k}}\right) \\ + \sum_{k=-\infty}^{\infty} 2J_k(m)J_{k+1}(m)e^{-(\delta_k+\delta_{k+1})} \cos\left[\omega_m t - (\phi_k - \phi_{k+1})\right] \\ + \sum_{k=-\infty}^{\infty} 2J_k(m)J_{k+2}(m)e^{-(\delta_k+\delta_{k+2})} \cos\left[2\omega_m t - (\phi_k - \phi_{k+2})\right] \\ + \sum_{k=-\infty}^{\infty} 2J_k(m)J_{k+3}(m)e^{-(\delta_k+\delta_{k+3})} \cos\left[3\omega_m t - (\phi_k - \phi_{k+3})\right] \\ + \ldots\ldots \end{array} \right\}. \quad (6)$$

The light absorption intensity contains many sidebands of first, second, third … harmonics, whose amplitudes can be demodulated by the corresponding reference frequencies in the mixer and LIA [8]. (In our setup (Fig. 1), only one set of the mixer and the LIA is utilized to deduce the first-derivative signal.) The first-derivative signal for carrier frequency $\omega 0$ or the amplitude of the $\cos\omega mt$ in Eq. (6) becomes

$$\frac{\partial I_{PD}}{\partial \omega_0} = 2k_{LIA}E_0^2 \times \sum_{k=0}^{\infty} J_k(m)J_{k+1}(m) \left[e^{-(\delta_k+\delta_{k+1})} - e^{-(\delta_{-k}+\delta_{-k-1})}\right], \quad (7)$$

where k_{LIA} is the LIA coefficient.

The first-derivative signal given by Eq. (7) is an odd function, which becomes zero when the laser carrier

frequency and the center frequency of an absorption line are matched. Therefore, this signal can be used as an error signal to lock the laser frequency at the selected absorption line with a PID controller as shown in Fig. 1.

Residual amplitude modulation

In SPM that uses an EOM, the main causes of the RAM are the etalon effect and the mismatch of the polarization axis of the laser beam with the EOM crystal [9, 10]. The first cause of the RAM is the etalon effect. Due to the reflectivity of the crystal surface, a part of the incident light is multi-reflected inside the EOM and generate etalon interference, which originates RAM (Fig. 2). The second cause is the mismatch between the polarization plane of the laser beam and the voltage-applied axis of the crystal (x-axis). In this condition, the part of propagated light, which has polarization plane on the y-axis, has different phase-shift from that on the x-axis. The phase-shift difference of the two light beams originates an intensity change of the output light that results in RAM. The RAM error depends on laser beam polarization, the DC-offset applied to the EOM, which may change the birefringent effect [9], and the EOM temperature, which may change refractive index and length of the crystal [20].

By defining the amplitude/phase modulation ratio and phase shift as r_{AM} (RAM coefficient) and ϕ_{AM}, respectively, the EOM-modulated electrical field (Eq. (1)) is rewritten as [8, 26].

$$E_{EOM} = E_0[1 + r_{AM}\cos(\omega_m t + \phi_{AM})] \exp\{-i(\omega_0 t + m\sin\omega_m t)\}. \tag{8}$$

The phase ϕ_{AM} can be calculated using the Fabry-Perot equation for an etalon [9] as

$$\phi_{AM} = \arctan\left(\frac{R\sin\phi_0}{1 - R\cos\phi_0}\right), \tag{9}$$

where R is the reflectivity coefficient and ϕ_0 is the original phase of the input laser beam. Assume that $\phi_0 = 0$, then $\phi_{AM} = 2\pi$ [rad] and the absorption signal I_{PD} (Eq. (6)) is corrected as

$$I_{PDRAM} = E_0^2(1 + 2r_{AM}\cos\omega_m t) \times \left\{ \begin{array}{c} J_0^2(m)e^{-2\delta_0} + \sum_{k=1}^{\infty} J_k^2(m)\left(e^{-2\delta_k} + e^{-2\delta_{-k}}\right) \\ + \sum_{k=-\infty}^{\infty} 2J_k(m)J_{k+1}(m)e^{-(\delta_k+\delta_{k+1})}\cos\left[\omega_m t - (\phi_k - \phi_{k+1})\right] \\ + \sum_{k=-\infty}^{\infty} 2J_k(m)J_{k+2}(m)e^{-(\delta_k+\delta_{k+2})}\cos\left[2\omega_m t - (\phi_k - \phi_{k+2})\right] \\ + \sum_{k=-\infty}^{\infty} 2J_k(m)J_{k+3}(m)e^{-(\delta_k+\delta_{k+3})}\cos\left[3\omega_m t - (\phi_k - \phi_{k+3})\right] \\ + \ldots\ldots \end{array} \right\}. \tag{10}$$

Equation (10) can be simplified as

$$I_{PDRAM} = I_{PD} + \Delta I_{RAM}, \tag{11}$$

where I_{PD} is the photo detector signal without RAM shown in Eq. (6), and ΔI_{RAM} is the RAM error component.

$$\Delta I_{RAM} = 2E_0^2 r_{AM}\cos\omega_m t \times \left\{ \begin{array}{c} J_0^2(m)e^{-2\delta_0} + \sum_{k=1}^{\infty} J_k^2(m)\left(e^{-2\delta_k} + e^{-2\delta_{-k}}\right) \\ + \sum_{k=-\infty}^{\infty} 2J_k(m)J_{k+1}(m)e^{-(\delta_k+\delta_{k+1})}\cos\left[\omega_m t - (\phi_k - \phi_{k+1})\right] \\ + \sum_{k=-\infty}^{\infty} 2J_k(m)J_{k+2}(m)e^{-(\delta_k+\delta_{k+2})}\cos\left[2\omega_m t - (\phi_k - \phi_{k+2})\right] \\ + \sum_{k=-\infty}^{\infty} 2J_k(m)J_{k+3}(m)e^{-(\delta_k+\delta_{k+3})}\cos\left[3\omega_m t - (\phi_k - \phi_{k+3})\right] \\ + \ldots\ldots \end{array} \right\}. \tag{12}$$

Because $r_{AM} << 1$, the terms with $(r_{AM}\cos\omega_m t)^2$ are neglected in Eq. (10). The combination of the RAM

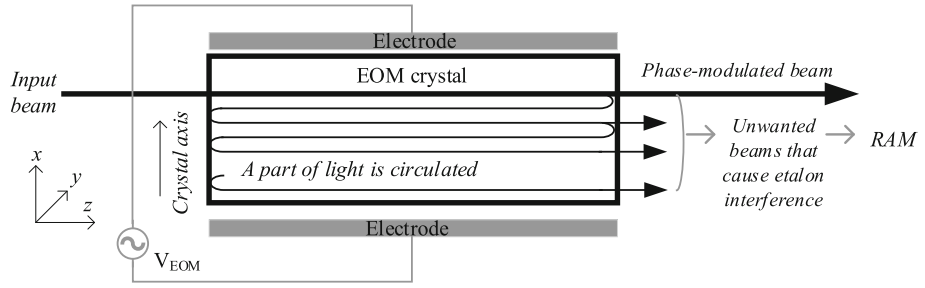

Fig. 2 The laser beam passes through an EOM crystal. The RAM is caused by the etalon effect of the laser beam and the EOM crystal

with the other harmonics generates new sidebands that contain the coefficient r_{AM} and causes errors in the absorption-derivative signals. For example, for the first-derivative signal, the RAM error originates from the product of the term of RAM with the DC and the second-harmonic terms, and the LIA signal or the first-derivative signal for ω_0 is corrected as

$$\frac{\partial I_{PDRAM}}{\partial \omega_0} = \frac{\partial I_{PD}}{\partial \omega_0} + \frac{\partial \Delta I_{RAM}}{\partial \omega_0}, \tag{13}$$

where $\frac{\partial I_{PD}}{\partial \omega_0}$ is the first-derivative signal without RAM that was shown by Eq. (7) in "Frequency modulation spectroscopy" section, and $\frac{\partial \Delta I_{RAM}}{\partial \omega_0}$ is from the RAM error calculated as

$$\frac{\partial \Delta I_{RAM}}{\partial \omega_0} = 2E_0^2 k_{LIA} r_{AM} \left\{ \begin{array}{l} J_0^2(m)e^{-2\delta_0} + \sum_{k=1}^{\infty} J_k^2(m)\left(e^{-2\delta_k} + e^{-2\delta_{-k}}\right) + \\ + \sum_{k=0}^{\infty} J_k(m)J_{k+2}(m)\left[e^{-(\delta_k+\delta_{k+2})} + e^{-(\delta_{-k}+\delta_{-k-2})}\right] \end{array} \right\}. \tag{14}$$

The relationship between the absorption signal and the first-derivative signal without RAM error (Eq. (7)) and the first-derivative signal with the RAM error obtained by simulation (Eqs. (13) to (16)) are shown in Fig. 3. The simulation conditions are shown in Table 1, which is based on our previous measurement [4].

In Fig. 3, the null point of the first-derivative signal, at which the laser frequency is locked, is shifted from the center frequency of the absorption line for ~ 0.035 and 0.5 MHz with $r_{AM} = 0.1$ and 2%, respectively. Since the RAM exists and the coefficient r_{AM} varies from 0 to 2% owing to environmental changes, the LD frequency is unstable with a maximum instability of $\sim 10^{-9}$. It is noted that, the RAM level is not necessary to be eliminated but need to be constant for a frequency stabilized LD. And under a well stable environment, the RAM fluctuation can be smaller than its maximum value of 2%, for example, with RAM fluctuation of 0.5%, the stability of 10^{-10} order can be achieved. However, since the RAM can be randomly fluctuated by environmental effects, it should be locked to some reliable point, such as the elimination point. The simulation shows that the RAM error can significantly reduce the frequency stability of iodine-frequency-stabilized LDs and limit their application in high-precision engineering.

From Eqs. (6) to (10), higher derivative orders such as the third-derivative signal can also be determined. Theoretically, the third-derivative signal is better for eliminating the Doppler background [6]; however, the RAM error, which originates from the products of RAM with the second and fourth-harmonic terms, also affects the third-derivative signal of the absorption lines. Finally, for the high-frequency stabilization of LDs, a compensation technique to eliminate the RAM is necessary.

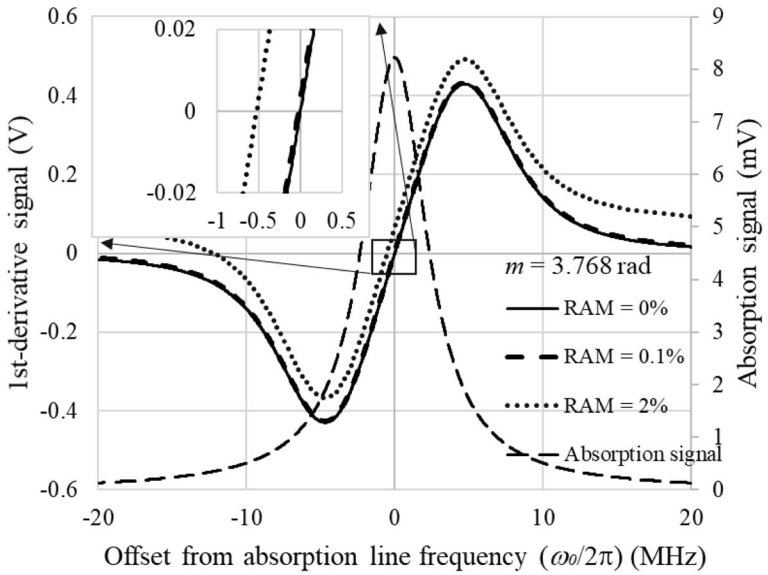

Fig. 3 The relationship between absorption signal, first-derivative signal (1st-dev.). The first-derivative is simulated with the RAM error of 0, 0.1, and 2%, respectively, the modulation index is fixed at 3.768 rad

Table 1 Simulation conditions

Carrier wavelength	632.9919 nm
EOM modulation frequency	1.5 MHz
EOM modulation index	3.768 rad
Absorption full-width at half maximum	3 MHz
RAM coefficient	0.02 and 0.001 (2 and 0.1%)
Absorption amplitude	0.3

RAM elimination methods

The RAM is originated from the etalon effect and the laser polarization mismatch with the EOM crystal axis [9, 10, 26]. For a passive method, the etalon effect can be reduced by tilting of the EOM crystal, but it can lead to more polarization-rotating error. The other passive method is utilizing a polarizer to correct the polarization of the input light. However, the RAM reduction is limited by the optics error, and the etalon effect cannot be neglected. Thereby, active methods are more efficient for RAM reduction. For the active method, the polarization mismatch can be minimized by adjusting the crystal optical axis using a DC-offset applied to the EOM [10]. The etalon effect can be eliminated by controlling optical path inside the EOM to an off-resonance condition with the laser beam. In this method, the optical path inside of the EOM is adjusted by the temperature through its relationship with the refractive index and thermal expansion of the crystal, and the applied DC-offset by a relation with the refractive index [27] as

$$\Delta n = \frac{1}{2} r_{33} V n_e^3 / d, \tag{15}$$

where r_{33}, V, d, and n_e are the birefringence coefficient, applied voltage, crystal thickness, and extraordinary refractive index, respectively. If a controllable DC-offset is added to the sinusoidal modulation signal and applied to the EOM, the crystal refractive index can be adjusted to eliminate the RAM.

The intensity modulated directly from the EOM can be detected by a photodetector placed immediately after the EOM. It can be expressed from Eq. (8) as

$$I_{EOM} = E_0^2[1 + r_{AM} \cos(\omega_m t + \phi_{AM})]^2. \tag{16}$$

If $r_{AM} = 0$, the first-order derivative of Eq. (16) obtained by a LIA synchronized with $\cos\omega_m t$ becomes null. The first-order derivative of Eq. (16) can be used for RAM suppression by a null method. The EOM

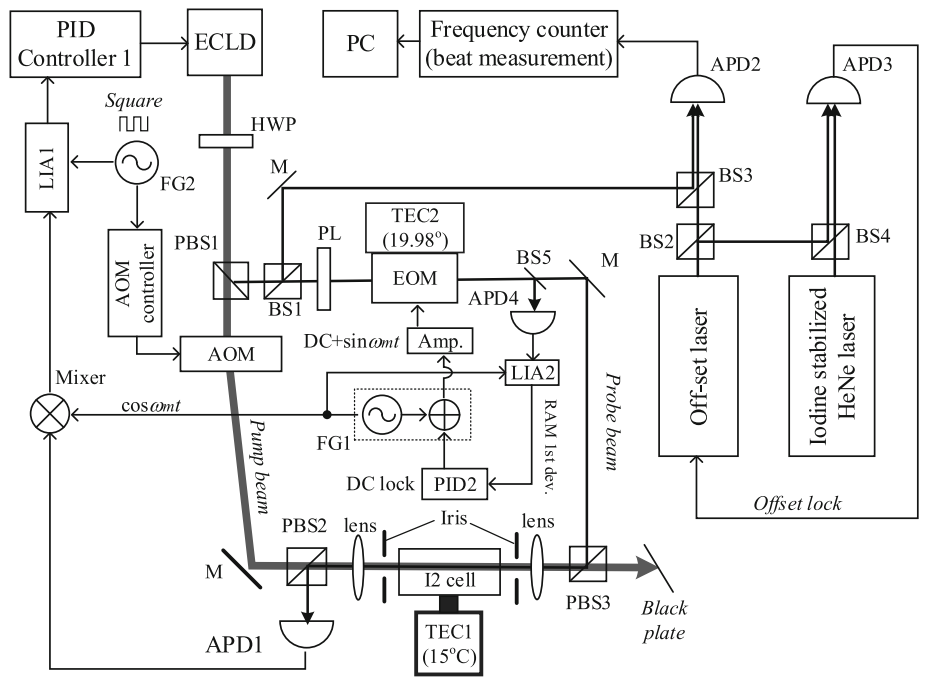

Frequency stabilization system

Fig. 4 The frequency stabilization system with RAM suppression. ECLD: external cavity laser diode; FG: function generator; PL: polarizer; EOM: electro-optic modulator; AOM: acousto-optic modulator; (P)BS: (polarizing) beam splitter; HWP: half-wave plate; APD: avalanche photodetector; TEC: thermoelectric cooler; LIA: lock-in amplifier

temperature is stabilized by a thermoelectric cooler (TEC). Then, the DC-offset voltage is adjusted by a fast PID controller to lock the first-derivative RAM signal (derivative with respect to $\omega_m t$ in Eq. (16)) to a null point and suppress the RAM.

Experiments

The LD frequency stabilization system with RAM suppression is shown in Fig. 4. In this system, an ECLD (TLM7000, New Focus) with an optical power of 2 mW and a linewidth of 300 kHz is employed as the laser source. The laser beam from the ECLD is split into a probe beam and a pump beam by a polarizing beam splitter (PBS) after passing through a half-wave plate (HWP). The HWP is rotated to adjust the power ratio between the pump and probe beams to 10/1. The pump beam with a higher power is frequency-shifted by 80 MHz and chopped with a 6.75 kHz square signal in an acousto-optic modulator (AOM, AOMO3080–125, Gooch & Housego). Then, it is fed through an iodine cell, which is kept at 15 °C, to saturate the internal environment of the cell. The probe beam polarization plane is adjusted by a polarizer (PL) and then phase-modulated by an EOM (4002, New Focus: half-wave voltage = 125 V at 633 nm) that is driven by a sinusoidal signal with a frequency of 1.5 MHz and a DC-offset from a function generator (FG1, WF1948, NF Corp.) and an EOM amplifier (3211, New Focus: amplifying gain = 40). The modulated beam is then fed to the iodine cell on the same line and in the opposite direction to the pump beam, then the saturated absorption signal is observed by an avalanche photodetector 1 (APD1, C5460, Hamamatsu). The overlapping of the two beams inside the iodine cell is ensured by two collimated lens and two pinholes. Since $1/e^2$ diameters of the pump and probe beams before lenses as shown in Fig. 4 are approximately 2 mm, and $1/e^2$ diameters of the focus points inside the iodine cell are approximately 1 mm, pinhole sizes for the pump and probe beams are approximately 2 and 1 mm, respectively. The experimental conditions are listed in Table 2.

From Eq. (16), the RAM coefficient can be measured as a half of the ratio between the AC (~ 0.105 V) and DC (~ 2.5 V) voltages in the APD4 (C5460, Hamamatsu) signal, and varies around 2% (≈0.5 × 0.105[V]/2.5[V]). In Fig. 4, the first-derivative RAM signal can be detected by LIA2 after APD4. Figures 5(a) and (b) show relationships between first-derivative RAM signal, EOM temperature, and DC-offset. As shown in Fig. 5(a), when the EOM is left under laboratory conditions for ~ 30 min and the DC-offset is 0 V, the temperature of the EOM is shifted by ~ 0.5 °C, the first-derivative RAM signal changed by a large amount, and at a temperature of ~ 19.98 °C, the RAM is minimized. In Fig. 5(b), when the EOM temperature is ~ 20.3 °C and the DC-offset applied to the EOM amplifier (amplifying gain = 40) is adjusted from − 3 to 3 V, we also see a periodic variation in the first-derivative RAM signal. The RAM is also eliminated when the DC-offset reaches ~ 0.9 and ~ 1.8 V.

To suppress the RAM, a combination method is employed using a thermoelectric cooler (TEC 3–6, ThorLAB) and a thermistor (TH10K, ThorLAB) to control the EOM temperature and the DC-offset is added to the FG1 signal directly. Since the slow control of the EOM temperature reduces the RAM fluctuation due to thermal drift, the DC-offset control works as a fast controller to eliminate the RAM. Figure 6 shows the temperature actuator for the commercial EOM with inexpensive TEC/thermistor. The TEC is attached to the aluminum case of the commercial EOM, and a temperature controller (TED200,

Table 2 Experimental conditions. (LPF: low pass filter)

Carrier wavelength	632.9919 nm		
I_2 cell cold-finger temperature	15 °C	LIA1 LPF cutoff frequency	100 Hz
Room temperature	20 ± 0.5 °C	LIA1 sensitivity	5 mV
Room pressure	100,855 ± 10 Pa	LIA2 LPF cutoff frequency	100 Hz
EOM modulation frequency	1.5 MHz	LIA2 sensitivity	100 mV
EOM modulation index	3.768 rad	AOM frequency shift	80 MHz
AC voltage applied to EOM amplifier	3.748 V_{PP}	AOM chopping frequency	6.4 kHz
DC-offset voltage range applied to EOM amplifier	±3 V	PID parameters for frequency stabilization	$K_P = 0.01$, $K_I = 0.015$, $K_D = 0.0075$
EOM amplifier gain	40	PID parameters for RAM suppression	$K_P = 0.2$, $K_I = 0.025$, $K_D = 0.03$
ECLD scanning range	1 GHz		
ECLD scanning time	100 s		

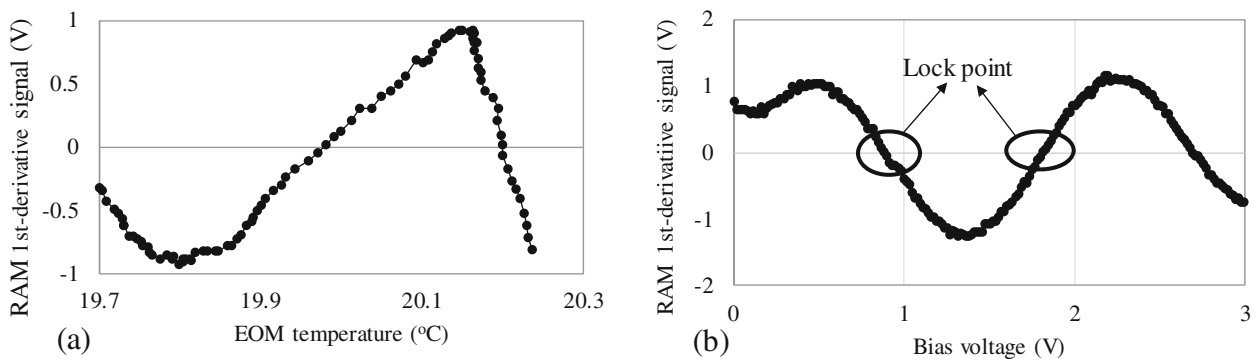

Fig. 5 The relationships between first-derivative RAM signal, EOM temperature, and DC-offset. **a** DC-offset is constant, EOM temperature changes; **b** EOM temperature is constant, DC-offset changes

ThorLAB) is utilized to stabilize the temperature of the EOM crystal at 19.98 °C.

Figure 7 shows RAM suppression procedure. In Fig. 7(a), the EOM temperature is stabilized first for approximately 45 min, then, a PID controller drives the DC-offset to lock the first-derivative RAM signal at a null point, where the RAM is suppressed (Fig. 7(b)). Figure 8 shows modulation signals that drive EOM, raw RAM signals detected by APD4 shown in Fig. 4 and fast Fourier transform (FFT) amplitudes of the raw RAM signals before and after RAM suppression. Before RAM suppression, the RAM coefficient r_{AM} is 0.02. After RAM suppression, the amplitude of the AC signal (1.5 MHz) of the photodetector is reduced to ~ 4.5 mV, and the DC signal of the photodetector is 2.5 V, the RAM coefficient r_{AM} is reduced to ~ 9×10^{-4} (= 0.5 × 0.0045 [V]/2.5 [V]).

To confirm the effect of the RAM on the first-derivative signal of the saturated absorption signal of the iodine molecule, the ECLD wavelength is scanned from ~ 632.9918 to ~ 632.9932 nm (approximately 1 GHz in the frequency domain) in 100 s, and the saturated spectrum of the P(33) transition that includes 21 absorption lines is detected. Figure 9 shows iodine molecule absorption (first-derivative) lines of the P(33) transition (a) before and (b) after RAM suppression. In Fig. 9(a), the absorption (first-derivative) signal is detected without RAM suppression. When the RAM variation is approximately 2% (10^{-2} order), the signal background contains more noise and the average line (dashed line) is offset from the null line, then the zero-crossing points of the lines shift from the line center, as mentioned in "Residual amplitude modulation" section. After suppressing the RAM to 9×10^{-4}, the average line (dashed line) of the absorption signal is almost zero, and the zero-crossing points of each absorption line are corrected (Fig. 9(b)).

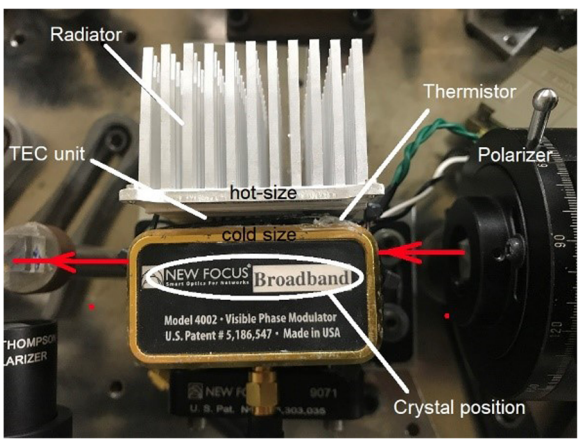

Fig. 6 Temperature actuator for the New Focus EOM4002 with inexpensive TEC/thermistor

After observing the first-derivative signal of the saturated absorption signal of the iodine molecule, the iodine-frequency-stabilized ECLD is examined with the iodine-stabilized He-Ne laser. Line b21, whose frequency is near the reference frequency of the iodine-stabilized He-Ne laser (NEO-92SI-NF, NEOARK), is selected to be the locking target for the PID controller for the precise detection of beat-note frequency. First, the ECLD frequency is scanned over ~ 50 MHz near line b21, and the first-derivative signal is obtained. The controller searches the null point of the derivative signal, then directly moves the ECLD frequency to the center of the absorption line. Subsequently, the PID controller with parameters tuned by the Nichols–Ziegler method [28] is activated to lock the first-derivative at the null point and stabilize the ECLD frequency at line b21. An ECLD laser beam is split before the EOM and sent to APD2 (C5658, Hamamatsu) to detect the beat-note frequency with the reference offset laser of the iodine-stabilized He-Ne laser as shown in Fig. 4. The He-Ne laser is locked at line a12 of the R(127) transition, and the laser offset is set at 300 MHz, then the

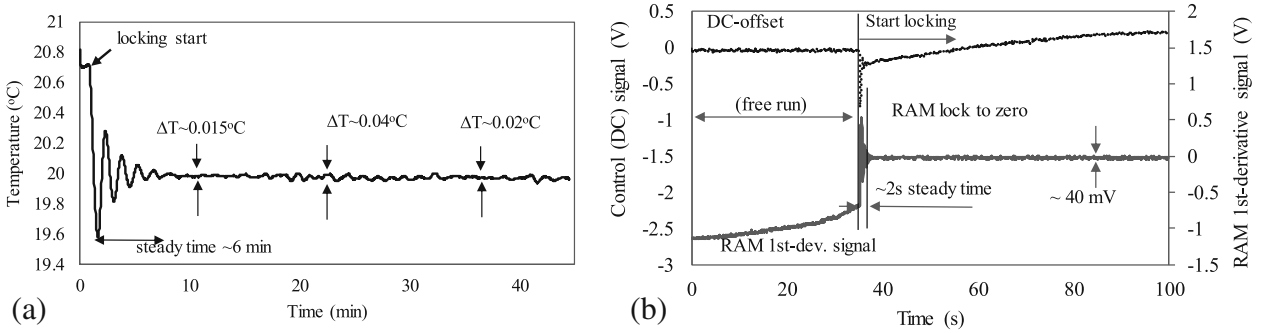

Fig. 7 RAM suppression procedure. **a** EOM temperature stabilization procedure (temporal change in EOM temperature) is performed first; and **b** DC-offset control procedure is examined for the first-derivative RAM signal suppression

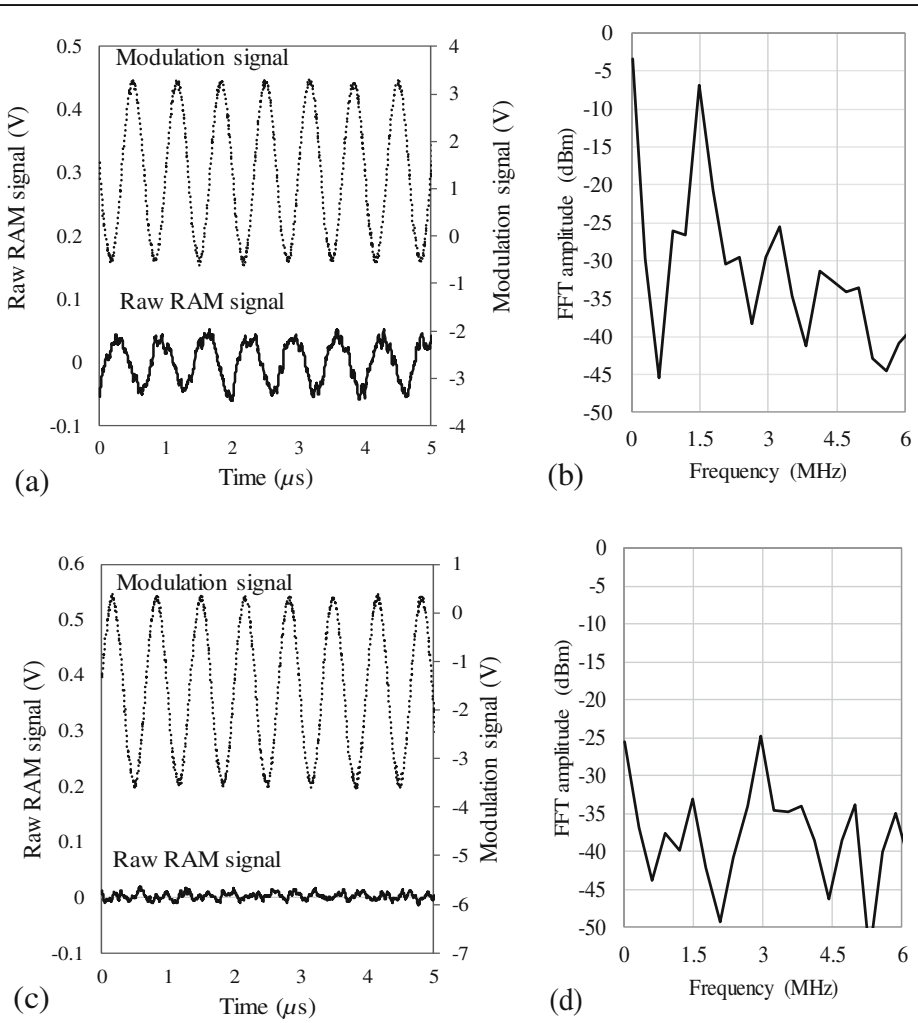

Fig. 8 RAM signals before and after suppression. **a**, **c** Modulation signals that drive EOM amplifier and raw RAM signals detected by APD4; **b**, **d** fast Fourier transform (FFT) amplitudes of the raw RAM signals; **a**, **b** Before suppression; **c**, **d** After suppression

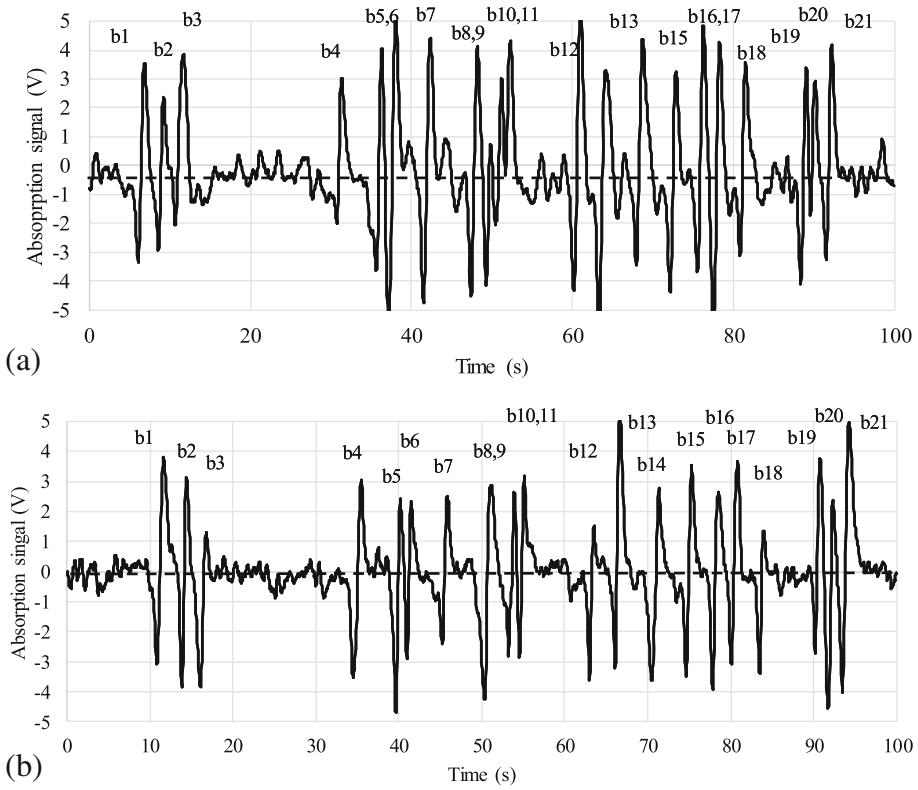

Fig. 9 Detected P(33) transition of the Iodine molecules absorption (first-derivative). **a** Before and **b** after RAM suppression (with both temperature and DC-offset controls). The background is almost null after RAM suppression. Dashed lines are the average lines for 100 s

beat-note frequency detected by a frequency counter (CNT-90, Pendulum) is ~ 645 MHz.

Results and discussion

Figure 10 shows beat-note frequencies measured between the iodine-frequency-stabilized ECLD before or after RAM suppression and the iodine-stabilized He-Ne laser and their Allan deviations. The PID control parameters and other conditions are the same in the two experiments. The Allan deviations for the beat-note signals with and without RAM suppression (includes both temperature and DC-offset controls) are shown in Fig. 1(b) and (d), respectively. Figure 10(a) and (c) show the highest stabilities of $\sim 1 \times 10^{-10}$ and $\sim 3.67 \times 10^{-11}$ for a sampling time of 1000 s before and after RAM suppression, with RAM coefficients of 10^{-2} and 9×10^{-4}, respectively.

Before RAM suppression, the frequency stability of $\sim 1 \times 10^{-10}$ can be achieved, that means the RAM fluctuation is smaller than its maximum of 2%. According to our simulation shown in Fig. 3, the 10^{-10} order of frequency stability corresponds to a RAM fluctuation of ~ 0.5% (10^{-3} order). Thereby, even though the RAM is reduced by ~ 20 times, the RAM fluctuation reduction is approximate five times. And due to the limited stability of the reference laser, we can only achieve the LD frequency stability at 10^{-11} order. The highest stability of the frequency-stabilized LD after RAM suppression is of almost same order as that of the iodine-stabilized He-Ne laser (frequency uncertainty $\sim 2.5 \times 10^{-11}$). The short-term (less than 10s) instability of the beat-note signal might be caused by the noise of the beat-note measurement, the linewidth of the LD, and environmental effects. However, by comparing Fig. 10(b) and (d), the short and long-term stability are observed to be improved by RAM suppression. This suggests that RAM suppression should be utilized for the frequency stabilization of LDs for displacement measurement, which uses sinusoidal phase modulation by an EOM.

Conclusions

In this study, the RAM effect of an EOM on a frequency stabilized LD to an iodine-saturated absorption line using FMS and an EOM is discussed. Then, we introduce a RAM compensation based on an EOM temperature stabilization and a DC-offset control. The RAM can be reduced to $\sim 9 \times 10^{-4}$, and the frequency stability of the ECLD reaches $\sim 1 \times 10^{-10}$ and $\sim 3.67 \times 10^{-11}$ for a sampling time of 1000 s, before and after RAM suppression, respectively. This RAM suppression is simple to be utilized with FMS system that uses any commercial EOM,

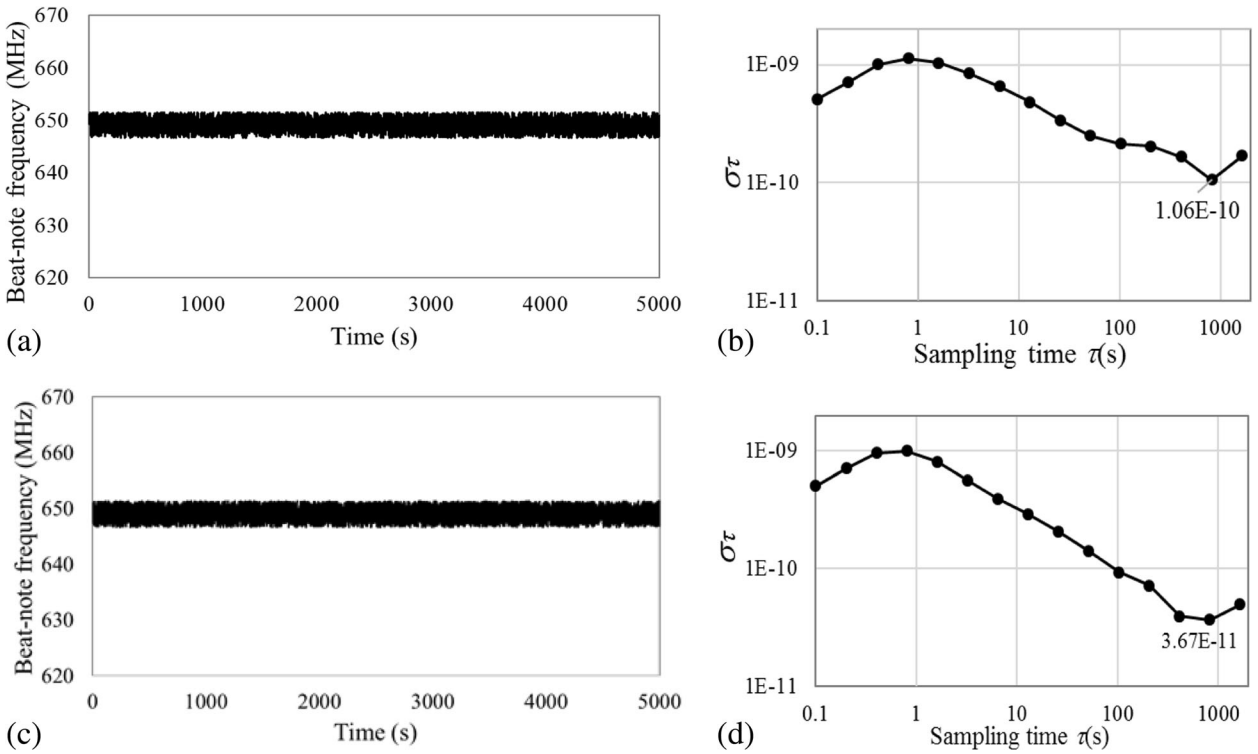

Fig. 10 ECLD frequency stability before and after RAM suppression. **a**, **c** Beat-note frequencies between the ECLD and the reference laser; **b**, **d** Allan deviations; **a**, **b** Before RAM suppression; **c**, **d** After RAM suppression

and the archived LD frequency stability is sufficient for most standard applications of displacement measuring interferometers [4]. By comparing Nd.YAG lasers with frequency stability of 10^{-12} order [7] and 10^{-14} order [29], or a femtosecond frequency comb with frequency stability of 10^{-14} order [30] with the developed ECLD, the frequency stability of the ECLD is typically low. In our future work, we also plan to use MTS to improve frequency stability using LD (DBR or DFB) with high power (10~20 mW). In another future work, the improvement of the displacement-measuring interferometer with the RAM suppression will be discussed.

Abbreviations

AOM: Acousto-optic modulator; APD: Avalanche photodetector; DBR: Distributed Bragg reflector; DFB: Distributed feedback; ECLD: External cavity laser diode; EOM: Electro-optic modulator]; FFT: Fast Fourier transform; FG: Function generator; FMS: Frequency modulation spectroscopy; HWP: Half-wave plate; LD: Laser diode; LIA: Lock-in amplifier; MTS: Modulation transfer spectroscopy; PBS: Polarizing beam splitter; PID: Proportional–integral–derivative; PL: Polarizer; RAM: Residual amplitude modulation; SFM: Sinusoidal frequency modulation; SPM: Sinusoidal phase modulation; TEC: Thermoelectric cooler

Acknowledgments

We express our gratitude to the Research Fund of Japan Society for the Promotion of Science for supporting this research. We would also like to thank Chuo Precision Industrial Co. Ltd., for valuable discussions.

Funding

Declared at acknowledgments.

Availability of data and materials

Presented in the main paper.

Authors' contributions

QAD proposed the idea and the calculation, carried out the experiments, and wrote the manuscript. All co-authors participated in the discussion of the theory and experimental results. All authors read and approved the final manuscript.

Authors' information

Mr. Quang Anh DUONG received his BSc in Mechanical Engineering from the Hanoi University of Science and Technology, Vietnam, in 2010, and received his MSc in Mechanical Engineering from the Nagaoka University of Technology, Japan, in 2013. He is now a Doctor candidate in the Department of Information Science and Control Engineering at the Nagaoka University of Technology, Japan. His interest includes applied optics, precision engineering and control science.

Mr. Thanh Dong NGUYEN received his BSc and MSc in Engineering from the Hanoi University of Science and Technology, Vietnam, in 2010 and 2013, respectively. He is now a Doctor candidate in the Department of Information Science and Control Engineering at the Nagaoka University of Technology, Japan. His interest includes precision engineering, applied optics and intelligent signal processing.

Dr. Thanh Tung VU received his BSc and MSc in Engineering from the Hanoi University of Science and Technology of Vietnam, in 2009 and 2011, respectively, and he received his Doctor of Engineering from the Nagaoka University of Technology, Japan, in 2016. He is now a lecturer and a researcher at the Department of Precision Mechanical and Optical Engineering, School of Mechanical Engineering, Hanoi University of Science and Technology, Vietnam. His research interests are applied optics, precision engineering and smart sensors.

Mr. Masato HIGUCHI received his BSc and MSc in Mechanical Engineering from the Nagaoka University of Technology in Japan, in 2015 and 2017, respectively. Now he is a Doctor candidate student in the Department of Information Science and Control Engineering at the Nagaoka University of Technology.
Dr. Dong WEI received his BSc and MSc in Engineering from the University of Electro-Communications of Japan, in 2006 and 2008, respectively, and he received his Doctor of Engineering from the University of Tokyo, Japan, in 2011. He is now an assistant professor in the Department of Mechanical Engineering at Nagaoka University of Technology of Japan. His interest includes applied optics and intelligent signal processing.
Prof. Dr. Masato AKETAGAWA received his Bachelor of Science and Master of Science from Department of Applied Physics at Tokyo Institute of Technology, Japan, in 1983 and 1985, respectively. He joined Canon Company from 1985 to 1990 as a researcher of Excimer laser lithography equipment. After that, he joined Nagaoka University of Technology. He received his Doctor of Engineering from Nagaoka University of Technology in 1997. He is now a Professor of Department of Mechanical Engineering. He is interested in applied physics, precision machinery, precision engineering, scanning probe microscope, optical interferometer, and especially picometer measurement.

Competing interests
The authors declare that they have no competing interests.

Publisher's Note

Author details
[1]Department of Mechanical Engineering, Nagaoka University of Technology, 1603-1 Kamitomioka, Nagaoka, Niigata 940-2188, Japan. [2]School of Mechanical Engineering, Hanoi University of Science and Technology, 1 Dai Co Viet Road, Ha Noi, Viet Nam.

Received: 24 June 2018 Accepted: 22 October 2018
Published online: 06 November 2018

References
1. Kobayashi, T., Akamatsu, D., Hosaka, K., Inaba, H., Okubo, S., Tanabe, T., Yasuda, M., Onae, A., Hong, F.L.: Compact iodine-stabilized laser operating at 531 nm with stability at the 10^{-12} level and using a coin-sized laser module. Opt. Express. **23**, 20749–20759 (2015)
2. Bruner, A., Mahal, V., Kiryuschev, I., Arie, A., Arbore, M.A., Fejer, M.M.: Frequency stability at the kilohertz level of a rubidium-locked diode laser at 192.114 THz. Appl. Opt. **37**, 6410–6414 (1998)
3. Bertinetto, F., Cordiale, P., Galzerano, G., Bava, E.: Frequency stabilization of DBR diode laser against Cs absorption lines at 852 nm using the modulation transfer method. IEEE Trans. Instrum. Meas. **50**, 490–492 (2001)
4. Duong, Q.A., Vu, T.T., Higuchi, M., Wei, D., Aketagawa, M.: Iodine-frequency-stabilized laser diode and displacement-measuring interferometer based on sinusoidal phase modulation. Meas. Sci. Technol. **29**(6), 065204 (2018)
5. Vu, T.T., Maeda, Y., Aketagawa, M.: Sinusoidal frequency modulation on laser diode for frequency stabilization and displacement measurement. Measurement. **94**, 927–933 (2015)
6. Vu, T.T., Higuchi, M., Aketagawa, M.: Accurate displacement-measuring interferometer with wide range using an I_2 frequency-stabilized laser diode based on sinusoidal frequency modulation. Meas. Sci. Technol. **27**(10), 105201 (2016)
7. Arie, A., Schiller, S., Gustafson, E.K., Byer, R.L.: Absolute frequency stabilization of diode-laser-pumped Nd: YAG laser to hyperfine transition in molecular iodine. Opt. Lett. **17**, 1204–1206 (1992)
8. Reinhardta, S., Saathoff, G., Karpuk, S., Novotny, C., Huber, G., Zimmermann, M., Holzwarth, R., Udem, T., Hansch, T.W., Gwinner, G.: Iodine hyperfine structure and absolute frequency measurements at 565, 576, and 585 nm. Opt. Commun. **261**, 282–290 (2006)
9. Whittaker, E.A., Gehrtz, M., Bjorklund, G.C.: Residual amplitude modulation in laser electro-optic phase modulation. J. Opt. Soc. Am. B. **2**, 1320–1326 (1985)
10. Wong, N.C., Hall, J.L.: Servo control of amplitude modulation in frequency-modulation spectroscopy: demonstration of shot-noise-limited detection. J. Opt. Soc. Am. B. **2**(9), 1527–1533 (1985)
11. Shirley, J.H.: Modulation transfer processes in optical heterodyne saturation spectroscopy. Opt. Lett. **7**, 537–539 (1982)
12. McCarron, D.J., King, S.A., Cornish, S.L.: Modulation transfer spectroscopy in atomic rubidium. Meas. Sci. Technol. **19**(10), 105601 (2008)
13. Burck, F.D., Lopez, O.: Correction of the distortion in frequency modulation spectroscopy. Meas. Sci. Technol. **15**, 1327–1336 (2004)
14. Jaatinen, E., Chartier, J.-M.: Possible influence of residual amplitude modulation when using modulation transfer with iodine transitions at 543 nm. Metrologia. **35**, 75–81 (1998)
15. Schuldt, T., Döringshoff, K., Reggentin, M., Kovalchuk, E.V., Gohlke, M., Weise, D., Johann, U., Peters, A., Braxmaier, C.: A high-performance iodine-based frequency reference for space applications. Proc. SPIE. **10564**, 105641N-1 (2017)
16. Makinouchi, S., Watanabe, A., Takasaki, M., Ohara, T., Ong, J.H., Wakui, S.: An evaluation of a modulated laser encoder. Precis. Eng. **35**, 302–308 (2011)
17. Ohara, T.: Scanning probe position encoder (SPPE): a new approach for high-precision and high-speed position measurement system. Proc. SPIE. **4344**, 52–561 (2001)
18. Li, L., Liu, F., Wang, C., Chen, L.: Measurement and control of residual amplitude modulation in optical phase modulation. Rev. Sci. Instrum. **83**, 043111 (2012)
19. Cooper, D.E., Watjen, J.P.: Two-tone optical heterodyne spectroscopy with a tunable lead-salt diode laser. Opt. Lett. **11**, 606–608 (1986)
20. Whittaker, E.A., Shum, C.M., Grebel, H., Lotem, H.: Reduction of residual amplitude modulation in frequency-modulation spectroscopy by using harmonic frequency modulation. J. Opt. Soc. Am. B. **5**, 1253–1256 (1988)
21. Tai, Z., Yan, L., Zhang, Y., Zhang, X., Guo, W., Zhang, S., Jiang, H.: Electro-optic modulator with ultra-low residual amplitude modulation for frequency modulation and laser stabilization. Opt. Lett. **41**, 5584–5587 (2016)
22. NEOARK Corp. NEO-92SI-NF iodine stabilized He-Ne laser: User manual. http://neoark.co.jp/en/index.php/laser-product/. Accessed 16 Oct 2018.
23. Gerstenkorn, S., Luc, P.: Atlas du spectre d'absorption de la molecule d'iode 15734–15756 cm^{-1}. Laboratoire Aim'e Cotton, CNRS II, Orsay, France (1977)
24. Snyder, J.J., Raj, R.K., Bloch, D., Ducloy, M.: High-sensitivity nonlinear spectroscopy using a frequency-offset pump. Opt. Lett. **5**, 163–165 (1980)
25. Supplee, J.M., Whittaker, E.A., Lenth, W.: Theoretical description of frequency modulation and wavelength modulation spectroscopy. Appl. Opt. **33**, 6294–6302 (1994)
26. Kokeyama, K., Izumi, K., Korth, W.Z., Lefebvre, N.S., Arai, K., Adhikari, R.X.: Residual amplitude modulation in interferometric gravitational wave detectors. J. Opt. Soc. Am. A. **31**, 81–88 (2014)
27. Roussey, M., Bernala, M.P., Courjal, N., Labeke, D.V., Baida, F.: Electro-optic effect exaltation on lithium niobate photonic crystals due to slow photons. Appl. Phys. Lett. **89**, 241110 (2006)
28. Ziegler, J.G., Nichols, N.B.: Optimum settings for automatic controllers. J. Dyn. Syst. Meas. Control. **115**, 220–222 (1993)
29. Bitou, Y., Sasaki, K., Iwasaki, S., Hong, F.L.: Compact I2-stabilized frequency-doubled Nd:YAG laser for long gauge block interferometer. Jpn. J. Appl. Phys. **42**, 2867 (2003)
30. Ye, J., Ma, L.S., Hall, J.L.: Molecular iodine clock. Phys. Rev. Lett. **87**, 270801–270804 (2001)